# Direct transformation from amorphous to crystalline calcium phosphate facilitated by motif-programmed artificial proteins

Toru Tsuji[a,b], Kazuo Onuma[c], Akira Yamamoto[d], Mayumi Iijima[e], and Kiyotaka Shiba[a,b,1]

[a]Division of Protein Engineering, Cancer Institute, Japanese Foundation for Cancer Research, Koto, Tokyo 135-8550, Japan; [b]Core Research for Evolutional Science and Technology, Japan Science and Technology Agency, and [c]Institute for Human Science and Biomedical Engineering, National Institute of Advanced Industrial Science and Technology, Central 6, 1-1-1 Higashi, Tsukuba, Ibaraki 305-8566, Japan; [d]Biotechnology Group, Incubation Center, PENTAX Corporation, Wako, Saitama 351-0101, Japan; and [e]Dental Materials and Technology, Asahi University School of Dentistry, 1851-1 Hozumi, Hozumi-Cho, Motosu, Gifu 501-0296, Japan

Edited by Jack W. Szostak, Massachusetts General Hospital, Boston, MA, and approved September 8, 2008 (received for review May 2, 2008)

**An animal's hard tissue is mainly composed of crystalline calcium phosphate. In vitro, small changes in the reaction conditions affect the species of calcium phosphate formed, whereas, in vivo, distinct types of crystalline calcium phosphate are formed in a well-controlled spatiotemporal-dependent manner. A variety of proteins are involved in hard-tissue formation; however, the mechanisms by which they regulate crystal growth are not yet fully understood. Clarification of these mechanisms will not only lead to the development of new therapeutic regimens but will also provide guidance for the application of biomineralization in bionanotechnology. Here, we focused on the peptide motifs present in dentin matrix protein 1 (DMP1), which was previously shown to enhance hydroxylapatite (HAP) formation when immobilized on a glass substrate. We synthesized a set of artificial proteins composed of combinatorial arrangements of these motifs and successfully obtained clones that accelerated formation of HAP without immobilization. Time-resolved static light-scattering analyses revealed that, in the presence of the protein, amorphous calcium phosphate (ACP) particles increased their fractal dimension and molecular mass without increasing their gyration radii during a short period before precipitation. The protein thus facilitated reorganization of the internal structure of amorphous particles into ordered crystalline states, i.e., the direct transformation of ACP to HAP, thereby acting as a nucleus for precipitation of crystalline calcium phosphate. Without the protein, the fractal dimension, molecular mass, and gyration radii of ACP particles increased concurrently, indicating heterogeneous growth transformation.**

biomaterials | biomineralization | crystal growth | protein engineering

Hydroxylapatite ($Ca_{10}(PO_4)_6(OH)_2$, HAP) is a major component of bone and teeth (1). Formation of HAP in vitro is readily affected by the small changes in reaction conditions (2–4), whereas, in vivo, it is formed under the robust biomineralization process. Various proteins have been proposed to be involved in the biomineralization of HAP (5–7). Dentin matrix protein1 (DMP1) is one of such biomineralization proteins, and the ablation of its gene results in bone malformation (8–11). He *et al.* (6) have shown that two peptide motifs identified in DMP1 [motif-A (ESQES) and motif-B (QESQSEQDS)] enhanced in vitro HAP formation when immobilized on a glass plate (6). Along with DMP1's motifs, several peptides and proteins have been shown to act as accelerators of HAP formation, and it has been suggested that these molecules mediate nucleation during crystal formation (12–14). The purpose of our experiment was to gain insight into the molecular mechanism by which the peptide motifs of DMP1 facilitate HAP formation through our synthetic approach (15). Because immobilization of a specimen poses impediments to time-resolved analyses, such as light-scattering photometry (16, 17), we first synthesized motif-programmed artificial proteins from the two DMP1 motifs, because their isolated clones were found to accelerate HAP formation without immobilization, and then investigated the effects of the proteins on HAP mineralization using time-resolved static light-scattering analyses, TEM observations, and Raman spectroscopy.

## Results and Discussion

In our motif-programming synthetic approach (15, 18, 19), we first extract one or more motifs from natural proteins and then express them in the context of an artificial polypeptide (Fig. 1). In this study, we created a library of motif-programmed proteins from DMP1 motifs [motif-A (ESQES) and motif-B (QESQSEQDS)], which were previously shown to enhance HAP formation when immobilized on a glass substrate (6), and selected 18 clones composed of various numbers of the motifs in different orders that were well-expressed in *Escherichia coli* and were soluble after purification (Table 1). To select clones able to enhance HAP formation without immobilization, we monitored the effects of the artificial proteins on pH during in vitro HAP formation (20). After mixing calcium and phosphate ions in the absence of additives, the pH of the solution held at ≈7.5–7.6 for ≈15 min and then rapidly dropped to ≈7.2, where it stabilized again (Fig. 2*A*). X-ray diffraction (XRD) analysis showed that during the first phase (pH 7.5–7.6), the solution was mainly composed of amorphous calcium phosphate (ACP), and during the third phase (pH 7.2), it was enriched with HAP (Fig. 2 *B* and *C*), suggesting that the rapid drop of the pH (the second phase) reflected the transformation from ACP to HAP.

We added selected concentrations of the 18 artificial proteins to the precipitation system and then monitored the pH of the reaction mixture. Among the proteins tested, #64, #68, and #72 shortened the first stable period; i.e., they entered the second phase earlier than a reference [Fig. 3 and supporting information (SI) Fig. S1]. To quantitatively evaluate this acceleration, we arbitrarily defined an "acceleration index" (described in Fig. 2 legend), and indices for the 18 proteins tested are summarized in Table 1. A higher acceleration index indicates earlier entrance into the second phase. We also observed that clones with higher acceleration indices had the ability to form crystalline calcium phosphate under conditions that otherwise do not allow crystal

Author contributions: T.T. and K.S. designed research; T.T., K.O., A.Y., and M.I. performed research; K.O. contributed new reagents/analytic tools; T.T., K.O., A.Y., and M.I. analyzed data; and T.T., K.O., and K.S. wrote the paper.

The authors declare no conflict of interest.

This article is a PNAS Direct Submission.

Freely available online through the PNAS open access option.

[1]To whom correspondence should be addressed. E-mail: kshiba@jfcr.or.jp.

This article contains supporting information online at www.pnas.org/cgi/content/full/0804277105/DCSupplemental.

© 2008 by The National Academy of Sciences of the USA

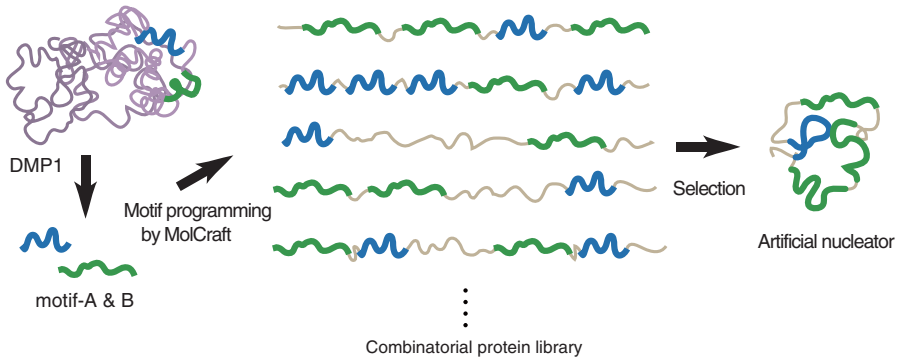


**Fig. 1.** Synthesis of artificial enhancer proteins for HAP mineralization from DMP1 motifs. Outline of motif-programming using MolCraft (18). The motifs are extracted from natural mineralization-related proteins (2 motifs in DMP1 (6) were used in this study) and embedded in different reading frames of a single microgene. The designer microgene is then polymerized to generate a library for artificial proteins that contain various numbers of the embedded motifs in different orders (described in detail in *SI Text*). Clones showing mineralization activity are then selected from this library.

formation, even after incubation for 10 days, and that this effect required the presence of the embedded motifs (Fig. S2, Table S1).

It was of interest to us that the mixture of pA and pB peptides (synthetic peptides of motif-A and B, respectively) had no effect on the formation of ACP or HAP, even at the high concentrations (Fig. 3), which is in contrast to a previous report describing the ability of these peptides to enhance those reactions (6). This discrepancy most likely reflects the different mobility state of the peptides in the present study. The previously reported accelerating activity of the peptides was observed with peptides immobilized on a solid substrate (6). By contrast, our assay permitted the peptides to move in solution. Similar contradictory effects that reflect the mobility state have also been reported for several acidic proteins, including DMP1 (6, 21). In our assay system, the parental DMP1 has delayed formation of HAP by extending the first phase (Fig. 3). In subsequent experiments we focused on the action of clone #64, which had the highest acceleration index, and asked how this protein accelerates HAP formation.

Time-resolved static light scattering (TR-SLS) measurements enabled us to observe changes in the apparent molecular mass ($M_w$), gyration radius ($R_g$), and fractal dimension ($d_f$) of calcium phosphate particles at an early stage during HAP formation (16, 17). Earlier studies that used conditions similar to the ones we used (1.0 mM $CaCl_2$ and 2.5 mM $KH_2PO_4$, pH 8.0 at 25 °C) revealed that ACP particles with radii ranging from 200 to 500 nm formed first in the solution (13, 17). Our conditions also produced initial particles having an $R_g$ of ≈340 nm and a $d_f$ of ≈1.8, irrespective of the presence of the #64. ACP particles with these $R_g$ and $d_f$ values persisted for ≈80–90 min [we called this "phase L" (L for latent)]. This period was followed a period of visual turbidity caused by a white precipitate (we called this "phase P") (Fig. 4*A*), which occurred earlier in the presence of #64 (after ≈93 min in the control vs. 83 min with #64). Notably, there was a short interval between phase L and phase P, during which the values of $M_w$, $R_g$, and $d_f$ showed distinct differences in

**Table 1. Summary of the artificial proteins created**

| Name | Structure | Molecular mass*, kDa | Isoelectric Point* | Acceleration index† |
|---|---|---|---|---|
| #55 | | 15.5 | 9.9 | 9 (25) |
| #56 | | 16.7 | 11.7 | 5 ( 5) |
| #57 | | 17.6 | 7.1 | 3 ( 5) |
| #58 | | 18.0 | 11.9 | 9 (0.2) |
| #59 | | 10.4 | 11.8 | 9 (25) |
| #60 | | 10.7 | 11.3 | 13 ( 5) |
| #61 | | 10.8 | 11.7 | 4 ( 5) |
| #62 | | 14.8 | 12.0 | 4 ( 1) |
| #63 | | 16.2 | 12.0 | 3 ( 5) |
| #64 | | 16.0 | 6.4 | 18.7 ± 2.1 (1) |
| #65 | | 16.9 | 11.8 | 9 (25) |
| #66 | | 18.0 | 11.2 | 7 (125) |
| #67 | | 18.4 | 11.8 | 10 (1) |
| #68 | | 15.0 | 10.8 | 18 (25) |
| #69 | | 16.2 | 10.7 | 5 (1) |
| #70 | | 16.1 | 12.2 | 0 (5) |
| #71 | | 12.5 | 11.9 | 4 (1) |
| #72 | | 12.8 | 10.4 | 17 (5, 25) |

*Calculated from deduced amino acids.

†Defined as described in Fig. 2*A*. The protein concentrations (μg/ml) that most strongly accelerated activity are indicated in parentheses. For #64, three independent experiments were performed and the data presented with standard deviation.

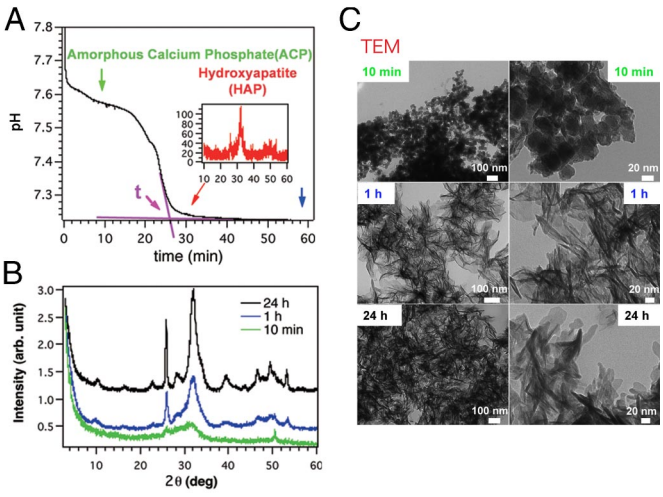


**Fig. 2.** The pH drop experiments. (*A*) pH-drop curve obtained during the precipitation of HAP from a solution of 2.0 mM $CaCl_2$ and 4.5 mM $KH_2PO_4$ (pH 8.0) without protein. A time, *t*, was defined at which a major pH change finished (pink arrow in *A*), and the acceleration index was defined as follows: Acceleration index = $[(t_{ref.} - t_{protein})/t_{ref}] \times 100$, where $t_{ref.}$ is the *t* when the solution does not contain proteins, and $t_{protein}$ is the *t* when the solution contains a particular protein. (*B*) XRD analysis of precipitates sampled 10 min, 1 h, and 24 h after the reaction was started. (*C*) TEM observations of the precipitate at the indicated times. (Scale bars: *Left*, 100 nm; and *Right*, 20 nm.)

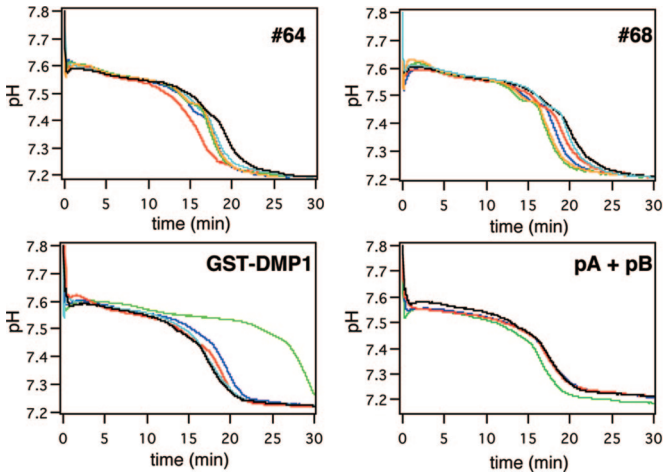


**Fig. 3.** pH-drop profiles in the presence of artificial proteins. pH changes were measured in the presence of different concentrations of the indicated proteins (sky blue, 0.2; red, 1; blue, 5; green 25; orange, 125 $\mu$g/ml).

#64-containing and control solutions (Fig. 4*B*). We called this short period "phase T," and it can be regarded as the nucleation step in this system. In the presence of #64, the values of $M_w$ and $d_f$ increased rapidly during phase T, but $R_g$ remained constant. Because $d_f$ is an index of the compactness of the inner structure of the particle, its increase means that the internal structure transformed from a comparatively loose (amorphous) to a closely packed (crystalline) structure, without an increase in radius. These changes in $M_w$ and $d_f$ are thus indicative of the transformation of ACP particles to crystalline particles. The $R_g$ remained nearly constant during phase T in the presence of #64 means that the amorphous-to-crystalline transformation proceeded via the "direct transformation" mode (17).

To confirm that the reorganization of ACP proceeded without an increase in size, we prepared freeze-dried samples of calcium phosphate deposits from phase L, phase T, and phase P and observed their sizes and ordered states. In the phase-L sample, spherical particles were discernible under TEM. Moreover, selected area electron diffraction (SAED) from the particles gave only a diffusive ring (Fig. 5*A*), indicating that the particles must be ACP. Raman spectroscopic analysis of the sample also indicated the ACP state of the sample (Fig. 6). The particles in the sample prepared from phase T were similar to phase L in their shapes (Fig. 5*B*), but SAED gave diffracted rings, which would not be observed with ACP. Unfortunately, incomplete diffraction hindered identification of the crystal species in the phase-T sample, but the Raman spectrum suggested the presence of HAP (Fig. 6). Thus, particles in the phase-T sample appear to have acquired an ordered structure without changing their size. In the sample from phase P, we observed well-grown HAP crystals whose identities were confirmed by SAED (Fig. 5*C*) and Raman spectroscopy (Fig. 6).

When we carried out the same analysis without #64, $M_w$, $R_g$, and $d_f$ all increased concurrently during phase T (Fig. 4*B*). The kinetics was well-described by the "heterogeneous growth-

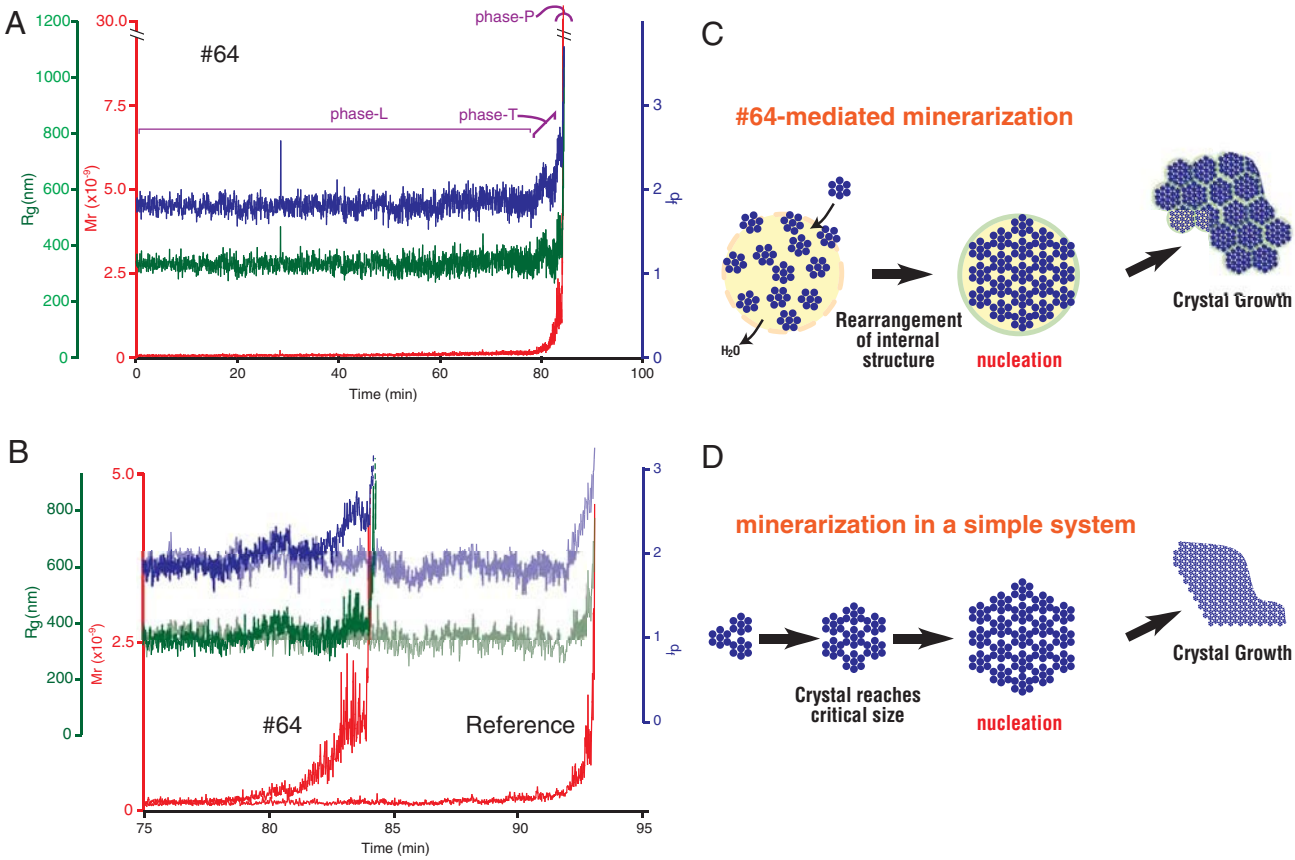


**Fig. 4.** TR-SLS measurements of calcium phosphate formation. (*A*) Time-dependent changes of the calculated apparent molecular mass ($M_w$, red), gyration radius ($R_g$, green), and fractal dimension ($d_f$, blue) of calcium phosphate in the presence of 1 $\mu$g/ml #64. Phases L, T, and P are explained in the text. (*B*) Enlargements corresponding to the period extending from minute 75 to minute 95 in *A*. For comparison, the data obtained in the absence of #64 are shown in light colors. (*C* and *D*) Schematic representation of HAP mineralization via direct transformation mediated by a protein (*C*) and in a simple system (*D*).

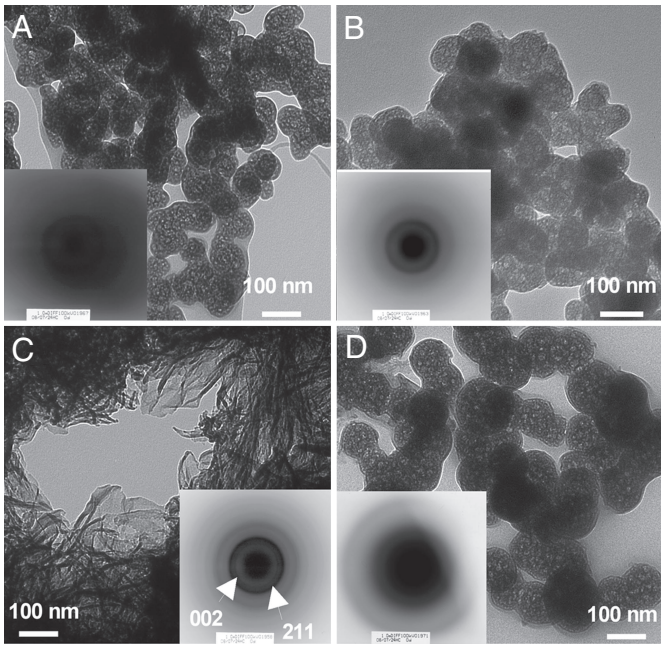


**Fig. 5.** Morphology and crystallinity of calcium phosphate particles appeared during precipitation experiments. (*A–C*) The freeze-dried samples were prepared from phase L (*A*), phase T (*B*), and phase P (*C*) in the presence of #64. (*D*) Sample was also prepared from phase P in the absence of protein.

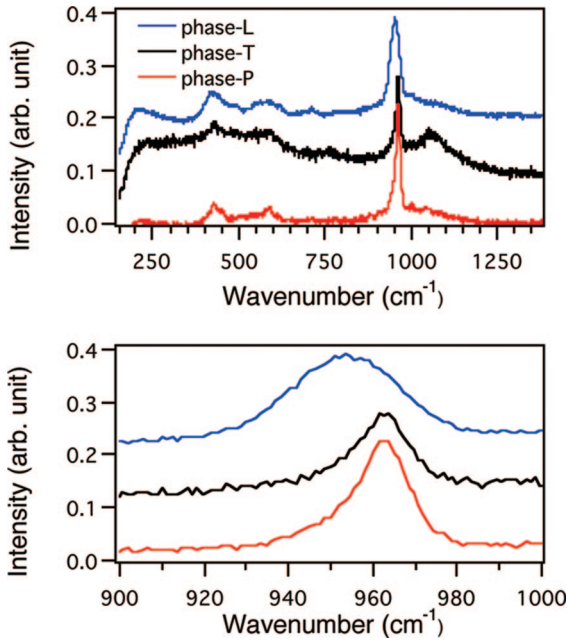


**Fig. 6.** Raman spectra of freeze-dried samples of phase L, phase T and phase P. The same samples used in Fig. 5 were analyzed by Raman spectrometer. The samples analyzed were prepared from phase L (blue), phase T (black) and phase P (red). The peak at 961 $cm^{-1}$ was typical to HAP (29). The broad spectrum from the phase-L sample suggested that it was composed of amorphous calcium phosphate.

transformation" model, which does not postulate direct transformation polymorphism (Fig. S3) (17). The freeze-dried particles prepared from a phase-P sample contained both HAP-like platelet particles (data not shown) and ACP-like spherical particles (Fig. 5*D*). In contrast to the spherical particles obtained from phase T of the #64 sample, these particles did not give diffracted rings on SAED, indicating they were still in an amorphous state. Thus, our data indicate that the presence of #64 altered the mode of nucleation during HAP formation.

Nucleation occurs at the point where the radius of a small but growing crystal reaches a critical size (critical radius) that then allows explosive growth of crystal (Fig. 4*D*). This critical value can be expressed as a function of the specific interfacial energy, volume of the growth units, supersaturation, and temperature (22). Although it is not known whether this relation can be simply applied to complex biomineralization systems, it has been proposed that biomolecules interact with the surfaces of embryonic crystals to reduce interfacial energy, resulting in smaller critical radius (6, 12, 23–25). As shown in earlier works (13, 17) and in the present study, compounds of calcium phosphate can exist as large (submicrometer sizes) amorphous particles for a period before being supplanted by large depositions of crystalline calcium phosphate. The transition period immediately preceding this explosive aggregation can be qualitatively regarded as the nucleation step. Two modes have been proposed for the transition from an amorphous to a crystalline structure: direct transformation and heterogeneous growth-transformation (17). Direct transformation postulates the reorganization of the internal structure of amorphous particles into ordered crystalline states, whereas heterogeneous growth transformation predicts that crystals grow incrementally on an amorphous groundwork, eventually overgrowing the preexisting amorphous particles. The data presented here indicate that an artificial protein containing biomineralization-related motifs is able to facilitate the direct transformation of submicrometer-sized amorphous particles into crystalline ones. Once these small crystalline particles are formed, they appear to explosively aggregate to form large crystals (Fig. 4 *C* and *D*), which we observed as the nucleation step on a macroscopic scale (Fig. 4*C*). Clarification of the mechanism by which proteins facilitate this transformation is our current interest. Constraint by proteins of the movement of water (and/or ions) clusters within the amorphous particles may be crucial for this transformation, as suggested from other biomineralization systems (26).

We are employing a synthesis approach to elucidate the function of motifs that are found in natural biomineralization proteins (15), which should fully complement reductionist approaches adopted in conventional molecular biology. Although a motif-based approach might reveal partial characters of parental protein (as shown in Fig. 3 and Fig. S4, the parental DMP-1 acted differently from motif peptides or synthetic proteins), this bottom-up approach should provide guidance for the application of biomineralization in bionanotechnology (27, 28).

## Materials and Methods

**Construction of Artificial Proteins.** The artificial proteins were created by using a MolCraft system (18). Briefly, a microgene was designed so that it encoded motif-A (QESQSEQDS) and motif-B (ESQES) in different reading frames and was then polymerized such that the reading frames changed randomly to generate a library of artificial proteins containing various numbers of the 2 motifs in different orders. These artificial proteins were then expressed in *E. coli* K12 strain XL1Blue (Stratagene), purified by using TALON resin (Clontech) under denaturing conditions, and dialyzed against 10 mM $KH_2PO_4$ (pH 8.0) or 1 mM HCl.

**Monitoring pH as an Index of HAP Precipitation.** Reactions were started by mixing of $KH_2PO_4$ solution (5.0 mM, 1,360 $\mu$l, pH 8.0) containing a certain amount of protein and $CaCl_2$ solution (21.3 mM, 140 $\mu$l) in a 2.0-ml plastic tube (Eppendorf) by using a magnet-stirring bar (6.35 × 3 mm). The pH of the solution was recorded every 1.5 s by using a pH meter (model F22; Horiba). Reactions were run at a constant temperature of 25 °C (Cool Stirrer SWC-900; Nissin).

**Time-Resolved Static Light-Scattering (TR-SLS) Measurements.** The solution used contained 2.5 mM $KH_2PO_4$ (adjusted to pH 8.0 by NaOH) and 1.0 mM $CaCl_2$, and the measurements were made at a constant temperature of 25 °C.

The apparent molecular mass ($M_w$), gyration radius ($R_g$) and fractal dimension ($d_f$,) were calculated as described in *SI Text*.

**Transmission Electron Microscopy (TEM) Observation and Raman Analyses.** The samples were centrifuged (16,000 × *g*, 25 °C, 0.5–3 min.), rinsed with 0.025% $NH_3$(aq) followed by dehydrated acetone (Wako), and freeze-dried. ACP particles might shrink during freeze-drying, because water molecules constituting the amorphous particles vaporized. The particles thus prepared were observed by TEM (H7600; Hitachi High Technologies) at 100 kV. The same samples were analyzed by using a Jasco NSR-1000 to obtain Raman spectra of calcium.

Additional data are presented in Figs. S5, S6, and S7 and in Table S2.

**ACKNOWLEDGMENTS.** We thank K. Takenouchi, Y. Iimori, and K. Yuba (PENTAX Corporation) for TEM and XRD measurements; T. Minamisawa and Dr. T. Akashi (Cancer Institute) for MS measurements; Dr. Kashiwagi (Cancer Institute) for his help in designing a microgene; Dr. M. Yudasaka (AIST) for Raman measurements; Drs. Y. Oaki and T. Saito and Prof. T. Kato (University of Tokyo) for helpful discussions and encouragement. This work was supported in part by Grant-in-Aid 18710164 for Young Scientists (B) from the Japan Society for the Promotion of Science (to T.T.).

1. Veis A (1989) in *Biomineralization Chemical and Biochemical Perspective*, eds Mann S, Webb J, Williams RJP (VCH, New York), pp 189–222.
2. Nancollas GH (1989) in *Biomineralization Chemical and Biochemical Perspective*, eds Mann S, Webb J, Williams RJP (VCH, New York), pp 157–187.
3. Eanes ED (2001) in *Octacalcium Phosphate*, eds Chow LC, Eanes ED (Karger, Basel), pp 130–147.
4. Iijima M, *et al.* (1991) Precipitation of octacalcium phosphate at 37 °C and pH 7.4 in relation to enamel formation. *J Cryst Growth* 112:467–473.
5. Hoang QQ, Sicheri F, Howard AJ, Yang DS (2003) Bone recognition mechanism of porcine osteocalcin from crystal structure. *Nature* 425:977–980.
6. He G, Dahl T, Veis A, George A (2003) Nucleation of apatite crystals in vitro by self-assembled dentin matrix protein 1. *Nat Mater* 2:552–558.
7. Margolis HC, Beniash E, Fowler CE (2006) Role of macromolecular assembly of enamel matrix proteins in enamel formation. *J Dent Res* 85:775–793.
8. Feng JQ, *et al.* (2006) Loss of DMP1 causes rickets and osteomalacia and identifies a role for osteocytes in mineral metabolism. *Nat Genet* 38:1310–1315.
9. Ling Y, *et al.* (2005) DMP1 depletion decreases bone mineralization in vivo: An FTIR imaging analysis. *J Bone Miner Res* 20:2169–2177.
10. Ye L, *et al.* (2005) Dmp1-deficient mice display severe defects in cartilage formation responsible for a chondrodysplasia-like phenotype. *J Biol Chem* 280: 6197–6203.
11. Ye L, *et al.* (2004) Deletion of dentin matrix protein-1 leads to a partial failure of maturation of predentin into dentin, hypomineralization, and expanded cavities of pulp and root canal during postnatal tooth development. *J Biol Chem* 279: 19141–19148.
12. Tarasevich BJ, *et al.* (2007) The nucleation and growth of calcium phosphate by amelogenin. *J Cryst Growth* 304:407–415.
13. Onuma K (2005) Effect of phosvitin on the nucleation and growth of calcium phosphates in physiological solutions. *J Phys Chem B* 109:8257–8262.
14. Hunter GK, Kyle CL, Goldberg HA (1994) Modulation of crystal formation by bone phosphoproteins: Structural specificity of the osteopontin-mediated inhibition of hydroxyapatite formation. *Biochem J* 300:723–728.
15. Shiba K, Minamisawa T (2007) A synthesis approach to understanding repeated peptides conserved in mineralization proteins. *Biomacromolecules* 8:2659–2664.
16. Becker A, Schmidt M (1991) *Macromol Chem Macromol Symp* 50:249–260.
17. Onuma K, *et al.* (2000) Precipitation kinetics of hydroxyapatite revealed by the continuous-angle laser light-scattering technique. *J Phys Chem B* 104:10563–10568.
18. Shiba K (2004) MolCraft: A hierarchical approach to the synthesis of artificial proteins. *J Mol Catalysis B* 28:145–153.
19. Saito H, *et al.* (2004) Synthesis of functional proteins by mixing peptide motifs. *Chem Biol* 11:765–773.
20. Ofir PBY, Govrin-Lippman R, Garti N, Füredi-Milhofer H (2004) The influence of polyelectrolytes on the formation and phase transformation of amorphous calcium phosphate. *Cryst Growth Des* 4:177–183.
21. He G, *et al.* (2005) Spatially and temporally controlled biomineralization is facilitated by interaction between self-assembled dentin matrix protein 1 and calcium phosphate nuclei in solution. *Biochemistry* 44:16140–16148.
22. Volmer M, Weber A (1926) Keimbidung in ubersattigten Gebilden (Nucleation of supersaturated structures). *Z Physik Chem* 119:277–301.
23. Addadi L, Weiner S (1989) Stereochemical and structural relations between macromolecules and crystals in biomineralization, eds Mann S, Webb J, Williams RJP (VCH, New York), pp 133–156.
24. Jiang H, Liu XY, Zhang G, Li Y (2005) Kinetics and template nucleation of self-assembled hydroxyapatite nanocrystallites by chondroitin sulfate. *J Biol Chem* 280:42061–42066.
25. Wu W, Zhuang H, Nancollas GH (1997) Heterogeneous nucleation of calcium phosphates on solid surfaces in aqueous solution. *J Biomed Mater Res* 35:93–99.
26. de la Rica R, Matsui H (2008) Urease as a nanoreactor for growing crystalline ZnO nanoshells at room temperature. *Angew Chem Int Ed Engl* 47:5415–5417.
27. Sano K, Shiba K (2008) In aqua manufacturing of a three-dimensional nanostructure using a peptide aptamer. *Mater Res Soc Bull*, 33: 524–529.
28. Aizenberg J, Muller DA, Grazul JL, Hamann DR (2003) Direct fabrication of large micropatterned single crystals. *Science* 299:1205–1208.
29. Koutsopoulos S (2002) Synthesis and characterization of hydroxyapaite crystals: A review study on the analytical methods. *J Biomed Mater Res* 62:600–612.